

# Spectral fluctuation analysis of ionospheric inhomogeneities over Brazilian territory Part II: E-F valley region plasma instabilities

Neelakshi J.<sup>1\*</sup>, Reinaldo R. Rosa<sup>1</sup>, Siomel Savio<sup>2,3,4</sup>, Francisco C. de  
Meneses<sup>3,5</sup>, Stephan Stephany<sup>1</sup>, Gabriel Fornari<sup>1</sup>, Muralikrishna P.<sup>2</sup>

<sup>1</sup>*Computational Space Physics Group, Lab for Computing and Applied Math (LABAC),  
National Institute for Space Research (INPE), Av. dos Astronautas, 1758, São José dos  
Campos, São Paulo, 12227-690, Brazil*

<sup>2</sup>*Aeronomy Division, National Institute for Space Research (INPE), Av. dos Astronautas,  
1758, São José dos Campos, São Paulo, 12227-690, Brazil*

<sup>3</sup>*China-Brazil Joint Laboratory for Space Weather, NSSC/INPE, Av. dos Astronautas,  
1758, São José dos Campos, São Paulo, 12227-690, Brazil*

<sup>4</sup>*State Key Laboratory of Space Weather, National Space Science Center (NSSC), Chinese  
Academy of Sciences, No. 1, Nanertiao, Zhongguancun, Haidian District, Beijing 100190,  
China*

<sup>5</sup>*School of Physics and Mathematics, Autonomous University of Nuevo León (UANL), Av.  
Universidad s/n, Cd. Universitaria, San Nicolás de los Garza, N.L. 66455, Mexico*

---

## Abstract

The turbulent-like process associated with ionospheric instabilities, has been identified as the main nonlinear process that drives the irregularities observed in the different ionospheric regions. In this complementary study, as proposed in the first article of this two-paper series [Fornari et al., Adv. Space Res. 58, 2016], we performed the detrended fluctuation analysis of the equatorial E-F valley region electron density fluctuations measured from an in situ experiment performed over the Brazilian territory. The spectral consistency with the K41 turbulent universality class is analyzed for E-F valley region from the DFA spectra for four electron density time series. A complementary detrended fluctuation analysis for four time series of the F-layer electric field is also presented. Consistent with the results obtained for the F region, the analysis for the E-F valley

---

\*Corresponding author: neelakshij@gmail.com

region also shows a very high spectral variation ( $\gg 50\%$ ). Thus, the spectral analysis performed in both parts of the series suggest that a process such as the homogeneous turbulence K41 ( $\beta = -5/3 \pm 2\%$ ) is inappropriate to describe both the fluctuations of electron density and the electric field associated with the main ionospheric instabilities.

*Keywords:* Equatorial ionospheric plasma irregularities, E-F valley region irregularities, detrending

---

## 1. Introduction

The characteristic features of in situ ionospheric plasma density fluctuation data may provide important information on the structural processes associated with ionospheric irregularities (Muralikrishna et al., 2003). In Part I of this work, Fornari et al. (2016) analyzed in situ F region electric field fluctuation data using the detrended fluctuation analysis (DFA) (Peng et al., 1994) technique to verify the wide variation in the spectral indices reported in earlier rocket experiments based on power spectral density (PSD) method. The results show that the high variability of the spectral indices is not due to the statistical limitation of the data, and does not constitute a K41 type of universality class<sup>1</sup>. As shown, in the first part of this study, PSD although widely used, falls short to characterize turbulence spectra from in situ ionospheric plasma density fluctuation measurements. Many studies have shown that the power spectra of these fluctuations exhibit two or three different spectral exponents indicating the scaling complexity of the process involved (Kelley and Hysell, 1991; Spicher et al., 2014). In general, the spectral indices that have been reported show deviation from the K41 theory but do not elucidate the statistical properties of

---

<sup>1</sup>The K41 is a theoretical framework for turbulence proposed by Kolmogorov in 1941, which forms a basis to understand the behavior of homogeneous multiplicative energy cascade from turbulent-like processes. Here the turbulent energy spectrum follows a precise power law behavior with index  $-5/3 \pm 2\%$  in the inertial range (Frisch, 1995). Therefore, the K41 spectrum represents a universality class for homogeneous turbulent processes.

the energy cascading that is supposed to drive the ionospheric turbulence (Kelley and Hysell, 1991). In this context, the DFA proposed by Peng et al. (1994) is a potential method that could render insights into the statistical properties of the turbulence phenomena.

As envisioned in Part I, here (Part II) the DFA is applied to in situ E-F valley region (hereafter, valley region) data. The valley region is located between the top of the E region and the base of the F region. The valley region, specifically the equatorial ones, hosts a variety of plasma irregularities both during the day, the so-called 150 km echoes (Kudeki and Fawcett, 1993; Rodrigues et al., 2011), and at dusk-nighttime (Chau and Hysell, 2004). This region is still a less explored area of research compared to the F region given the technical limitations in observing it. It can be studied by using powerful incoherent and coherent scatter radar and in situ experiments. Various studies have been reported on the correlation between the valley region irregularities and the equatorial plasma instabilities in the F region:

- Radar observations revealed that (i) the valley region irregularities are often found when the equatorial spread F (ESF) occurred after the sunset and that their spatial structures and temporal variations have resemblance with the ESF, and (ii) the valley region irregularities are a result of the coupling between the unstable equatorial F region and the underlying low-latitude valley and the E region (Vickrey et al., 1982, 1984; Patra, 2008; Yokoyama et al., 2005; Li et al., 2011; Kherani et al., 2012).
- Studies based on in situ data found that electric field and gravity waves may play a key role in the generation of these structures (in the valley regions) and that the structures are produced by the generalized Rayleigh-Taylor instability mechanism at the base of the F region (Vickrey et al., 1984; Prakash, 1999; Sinha et al., 1999; Muralikrishna et al., 2003; Savio et al., 2017). Savio et al. (2017) reported the presence of wave-like structures in valley region data obtained from an experiment over Brazil, and the same data is used for the present analysis.

In literature, the DFA is applied to study ionospheric irregularities, but we could not find its application to in situ valley region data. This work presents the first instance of application of the DFA to in situ E-F valley region electron density fluctuation data. The paper is organized as follows. Section 2 describes the data along with the electron density vertical profile. The DFA is presented in Section 3 followed by the concluding remarks in Section 4.

## 2. In situ valley region data

The vertical profile of electron density was obtained from a conical Langmuir probe on-board a two-stage VS-30 Orion sounding rocket experiment launched from an equatorial rocket launching station, Alcântara (2.24° S, 44.4° W, dip latitude 5.5° S), on December 8, 2012, at 19:00 LT, under quiet geomagnetic conditions. During the  $\sim 11$  min flight, rocket trajectory was in the north-northeast direction towards the magnetic equator, ranging  $\sim 384$  km horizontally with an apogee covering typical F region altitudes of  $\sim 428$  km. The conical Langmuir probe worked both in swept and constant bias modes. The probe sensor potential was swept from -1 V to +2.5 V linearly in about 1.5 s, during which the electron kinetic temperature was determined from the collected probe current. Then, the potential was maintained at +2.5 V (constant bias mode) for 1 s, during which the collected probe current was used to estimate electron density and its fluctuations, in each experiment cycle. This work utilizes the electron density fluctuation data obtained from the conical Langmuir probe. Fig. 1 shows variations in the vertically distributed electron density in the downleg (descent of the rocket) trajectory of the flight.

At the time of launch, the ground-based equipment detected conditions favorable for the generation of plasma bubbles in the F region. Savio et al. (2017) reported the presence of several small- and medium-scale plasma irregularities in the valley region (120-300 km) during both ascent and descent, which were more prominent during the descent of the rocket. In the downleg profile, the average electron density observed was around  $9 \times 10^9 m^{-3}$ , equivalent to 1/10th

of the E region maximum, and then, it gradually increased after 300 km, where the broad base of F region was detected. These observations are consistent with the work reported by Wakai (1967), which stated that under quiet conditions, the electron concentration in the valley around midnight is about 1/10th of the E region maximum, and width of the valley is very wide compared to the disturbed nights. Prakash et al. (1970) reported observing a deep valley region above 120 km, i.e., 120-140 km, where the electron density fell by two orders of magnitude in their experiment (to a few hundreds per cubic centimeters). Fig. 2 (left panel) shows the selected time series from the downleg electron density profile around average heights of 143, 205, and 263.9 km from the valley region and around 316.9 km, just above the wide base of the F region.

### **3. Fluctuation analysis, results and interpretation**

The DFA proposed by Peng et al. (1994) could render insights into the statistical properties of turbulence phenomena. Originally proposed to detect long-range correlations in DNA sequences and in data influenced by trends, the DFA is widely used in many branches of sciences - medicine, physics, finance and social sciences - to understand the complexity of systems through its scaling exponent that characterizes fractal dynamics of the system (Kantelhardt, 2009; Veronese et al., 2011).

The robustness of DFA can be attributed to some of its interesting features. For instance, Coronado and Carpena (2005) investigated the influence of the length of a time series in quantifying the correlation behavior using techniques like autocorrelation analysis, Hurst exponent, and DFA. The comparison study revealed that the DFA is practically unaffected by the length of time series, contrary to that observed from the results of Hurst analysis or autocorrelation analysis. Another interesting feature has been reported by Chen et al. (2002) who altered time series by excluding parts of it, stitching the rest and subjecting it to the DFA. The study revealed that even with the removal of 50% of the time series, the scaling behavior of positively correlated signals is unaltered,

implying that time series need not be continuous. Heneghan and McDarby (2000) established an equivalence relation between the PSD exponent,  $\beta$ , and the DFA exponent,  $\alpha$ , given by  $\beta \equiv 2\alpha - 1$ . Kiyono (2015) showed that this relationship is valid for the higher order DFA subject to the constraint  $0 < \alpha < m + 1$ , where  $m$  is the order of detrending polynomial in the DFA.

The DFA involves obtaining cumulative sum of the mean subtracted time series followed by dividing it into non-overlapping segments ( $s$ ), referred to as scales. Further, these segments are detrended using the linear least squares or higher order polynomial ( $m$ ) method and the variance is calculated. Depending on the detrending order,  $m$ , the analysis is referred to as DFA $m$ . Averaging the root mean square over the segments ( $s$ ) gives the fluctuation function,  $F(s)$ . Linear fit to the fluctuation function profile yields the scaling exponent  $\alpha$ . Implementation procedure can be found in Part I of this paper (Fornari et al., 2016). In this work, four time series of electron density fluctuations from the downleg profiles corresponding to the valley region are selected. The selected time series correspond to the mean heights of 143, 205, 263.9, and 316.9 km (please see left panel in Fig. 2).

The selected time series are subjected to DFA. Scales are varied from 10 to  $N/4$  with a factor of  $2^{\frac{1}{8}}$ , where  $N$  is the length of time series (Goldberger et al., 2000). The fluctuation function computed from DFA is plotted as a function of scales for all the selected time series (right panel in Fig. 2) on a log-log scale. The profiles of fluctuation function for all the chosen cases exhibit long-range correlation with a crossover. Crossover refers to a change in the scaling exponent for different scale ranges, and it usually arises due to a change in the correlation properties over different spatial or temporal scales, or from trends in the data. The exponents  $\alpha_1$  and  $\alpha_2$  are obtained from the linear fit of  $F(s)$ , where  $\alpha_1$  refers to smaller scales and  $\alpha_2$  refers to larger scales. Our analysis reveals  $\alpha_1$  to be in the range of 0.28 to 1.76 and  $\alpha_2$  in the range of 0.67 to 1.5. For mean heights corresponding to 143 and 205 km, we observe  $\alpha_1$  is smaller than  $\alpha_2$ , contrary to the observation for mean heights corresponding to 263.9 and 316.9 km.

In order to be sure that the obtained crossover is intrinsic to the data and not an artifact, we investigated the time series with higher order DFAs, of the order 1-5. For this investigation, we used the methodology prescribed by Kantelhardt et al. (2001) to identify false crossovers. Artificial crossover exhibits similar characteristic length with identical scaling. Fig. 3 presents the analysis for downleg time series corresponding to the mean height of 143 km with DFA of 1<sup>st</sup> to 5<sup>th</sup> order. The crossover exponents are listed in Table 1. It can be observed that as the order of detrending increases, crossover point moves towards larger scales and have different scaling exponents. This investigation confirms that the obtained crossover is an intrinsic property of electron density fluctuation data in the valley region.

The PSD exponent,  $\beta$ , is calculated using the equivalence relationship given above, and the standard deviation  $\sigma_m$  (in %) is determined. The computed DFA exponents in our analysis show a wide range of  $\beta$  from  $-0.98$  to  $-2.14$  with  $\sigma_m = 58\%$ . Table 2 summarizes the variations in the  $\beta$  exponent obtained from the previous equivalent studies (Rino et al., 1981; Kelley et al., 1982; Muralikrishna and Vieira, 2007; Sinha et al., 2010, 2011) and compares with the present work. All studies reported in Table 2 are based on electron density fluctuation data obtained through rocket experiments. It is observed that the computed standard deviation  $\sigma_m \gg 50\%$ , which affirms that the underlying mechanism for instabilities differs from the K41 homogeneous turbulence, given the accepted deviation is  $\sigma_m \leq 2\%$  (Frisch, 1995).

We also performed the DFA on in situ electric field fluctuation data from the F region obtained from an earlier experiment conducted on December 18, 1995, at 21:17 LT, under quiet geomagnetic conditions from the same equatorial launching station Alcântara ( $2.24^\circ$  S,  $44.4^\circ$  W, dip latitude  $5.5^\circ$  S) (Fornari et al., 2016). The rocket flight traversed through similar altitudes of 200-300 km. This data indicated the presence of a large plasma bubble at an altitude of  $\sim 280$  km. Fig. 4 presents the time series and the corresponding DFA.

The data from aforementioned experiments is selected for the altitudes of 200-300 km. In valley region data, small-to-medium scale plasma irregularities

(Savio et al., 2017) are found, while F-region data shows medium-to-large scale plasma irregularities (Fig. 2 in Muralikrishna et al., 2003). Hence, it will be interesting to compare the scaling exponents of plasma densities around similar altitudes for these two different regions. Fig. 5 shows the scaling exponent plotted as a function of height for the valley region (left panel) and the F region (right panel). For this plot, we have used a single linear fit for valley region data. The shaded horizontal bar in the plot represents the exponent value,  $\alpha = 1.33 \pm 2\%$ , for the homogeneous turbulence described by the K41 theory. The range of  $\alpha$  exponents for the F region is higher than that of the valley region, which may be due to different scaling present in these regions. Wide variations of the scaling exponent from the K41 theory are observed for both regions.

#### 4. Concluding remarks

In this paper, the complementary in situ E-F valley region irregularities are studied using the DFA. This study is important as studies of the equatorial E-F valley region at nighttime are scarce. Our analysis shows that the E-F valley region electron density fluctuations exhibit long-range correlation with crossovers that are intrinsic to the data for all the chosen altitudes. The F region irregularities obtained from an earlier experiment are also analyzed using the DFA and similar results in terms of long-range correlations are obtained for all the chosen altitudes. The PSD exponent  $\beta$  is computed for the current data and compared with earlier similar experiments. The results show  $\sigma_m \gg 50\%$ . These observations along with the profile of  $\alpha$  with respect to the height indicate that scaling exponents show wide variation from the K41 theory, for both the E-F valley and F regions. This implies that the turbulent-like ionospheric fluctuations as a whole cannot be described by the K41 homogeneous energy cascade theory.

Given this scenario and considering the different mechanisms responsible for the plasma instability along different ionospheric regions, it is necessary to inves-

tigate the model for non-homogeneous turbulence that will help to understand the observed high spectral variability. A future study that emerges naturally in this scenario is to look for multifractal signature from the data analyzed here. This investigation is in progress and will be published in an upcoming paper.

### **Acknowledgement**

The authors are grateful to the Institute of Aeronautics and Space (IAE/DCTA) and Alcântara Launch Center (CLA) for providing sounding rocket and launch operation, respectively. NJ acknowledges the financial assistance received from CAPES. RRR is grateful to FAPESP sponsored by Process No. 2014/11156–4. S.Savio acknowledges the financial support from China-Brazil Joint Laboratory for Space Weather, National Space Science Center, Chinese Academy of Science. F.C. de Meneses acknowledges the financial support given by the National Council of Science and Technology of Mexico (CONACYT), CAS-TWAS Fellowship for Postdoctoral and Visiting Scholars from Developing Countries under Grant no. 201377GB0001, and the Brazilian Council for Scientific and Technological Development (CNPq) under Grant number 312704/2015–1. S.Stephany thanks CNPq for grant 307460/2015-0

### **References**

### **References**

- Chau, J. L., and Hysell, D. L., 2004. High altitude large-scale plasma waves in the equatorial electrojet at twilight. *Ann. Geophys.*, 22, 4071-4076, <https://doi.org/10.5194/angeo-22-4071-2004>.
- Chen, Z., Ivanov, P. Ch., Hu, K., and Stanley, H. E., 2002. Effect of non-stationarities on detrended fluctuation analysis. *Phys. Rev. E*, 65, 041107, <https://doi.org/10.1103/PhysRevE.65.041107>.
- Coronado, A.V., and Carpena, P., 2005. Size effects on correlation measures. *J. Biol. Phys.*, 31, 121-133, <https://doi.org/10.1007/s10867-005-3126-8>.

- Fornari, G., Rosa, R., De Meneses, F. C. Jr., and Muralikrishna, P., 2016. Spectral fluctuation analysis of ionospheric inhomogeneities over Brazilian territory. Part I: Equatorial F-region plasma bubbles, *Adv. Space Res.*, 58, 2037-2042, <https://doi.org/10.1016/j.asr.2016.03.039>.
- Frisch, U. (1995) *Turbulence: The Legacy of A. N. Kolmogorov*. New York, Cambridge University Press.
- Goldberger, A. L., Amaral, L. A. N., Glass, L., Hausdorff, J. M., Ivanov, P. Ch., Mark, R. G., Mietus, J. E., Moody, G. B., Peng, Chung-Kang, and Stanley, H. E. (2000). PhysioBank, physioToolkit, and physionet: Components of a new research resource for complex physiologic signals. *Circulation*, 101, e215-e220, <https://doi.org/10.1161/01.CIR.101.23.e215>.
- Heneghan, C., and McDarby, G. (2000). Establishing the relation between detrended fluctuation analysis and power spectral density analysis for stochastic processes. *Phys. Rev. E*, 62, 6103-6110, <https://doi.org/10.1103/PhysRevE.62.6103>.
- Kantelhardt, J. W., Koscielny-Bunde, E., Rego, H. H. A., Havlin, S., and Bunde, A. (2001). Detecting long-range correlations with detrended fluctuation analysis. *Physica A*, 295, 441-454, [https://doi.org/10.1016/S0378-4371\(01\)00144-3](https://doi.org/10.1016/S0378-4371(01)00144-3).
- Kantelhardt, J. W. (2009). 'Fractal and multifractal time series' in Meyers, R. A. (ed.). *Encyclopedia of complexity and systems science*. Springer New York, 3754-3779, [https://doi.org/10.1007/978-0-387-30440-3\\_221](https://doi.org/10.1007/978-0-387-30440-3_221).
- Kelley, M. C., Pfaff, R. F., Baker, K. D., Ulwick, J. C., Livingston, R., Rino, C., and Tsunoda, R. (1982). Simultaneous rocket probe and radar measurements of equatorial spread-F-transitional and short wavelength results. *J. Geophys. Res.*, 87, 1575-1588, <https://doi.org/10.1029/JA087iA03p01575>.
- Kelley, M. C., and Hysell, D. L. (1991). Equatorial spread-F and neutral atmospheric turbulence: A review and a comparative anatomy. *J. Atmos. Terr. Phys.*, 53, 695-708, [https://doi.org/10.1016/0021-9169\(91\)90122-N](https://doi.org/10.1016/0021-9169(91)90122-N).

- Kherani, E. A., De Paula, E. R., Cueva, R. Y. C., and Camargo, L. A. P. (2012). Observations of nighttime equatorial-upper-E-valley region irregular structures from São Luís radar and their occurrence statistics: A manifestation of vertical coupling between E and F regions. *J. Atmos. Terr. Phys.*, 75-76, 64-70, <https://doi.org/0.1016/j.jastp.2011.08.017>.
- Kiyono, K. (2015). Establishing a direct connection between detrended fluctuation analysis and Fourier analysis. *Phys. Rev. E*, 92, 042925, <https://doi.org/10.1103/PhysRevE.92.042925>.
- Kudeki, E. and Fawcett, C. D. (1993). High resolution observations of 150 km echoes at Jicamarca. *Geophys. Res. Lett.*, 20, 1987-1990, <https://doi.org/10.1029/93GL01256>.
- Li, G., Ning, B., Patra, A. K., Wan W., and Hu, L. (2011). Investigation of low-latitude E and valley region irregularities: Their relationship to equatorial plasma bubble bifurcation. *J. Geophys. Res.*, 116, A11319, <https://doi.org/10.1029/2011JA016895>.
- Muralikrishna P., Vieira, L. P., and Abdu, M. A. (2003). Electron density and electric field fluctuations associated with developing plasma bubbles. *J. Atmos. Sol-Terr. Phy.*, 65, 1315-1327, <https://doi.org/10.1016/j.jastp.2003.08.010>.
- Muralikrishna, P. and Vieira, L. P. (2007). Equatorial F-region irregularities generated by the Rayleigh-Taylor instability mechanism - Rocket observations from Brazil. *Revista Brasileira de Geofísica, SciELO Brasil*, 25, 135-149, <https://doi.org/10.1590/S0102-261X2007000600016>.
- Patra A. K. (2008). Some aspects of electrostatic coupling between E and F regions relevant to plasma irregularities: A review based on recent observations. *J. Atmos. Sol-Terr. Phy.*, 70, 2159-2171, <https://doi.org/10.1016/j.jastp.2008.05.013>.

- Peng, C. K., Buldyrev, S. V., Havlin, S., Simons, M., Stanley, H. E., and Goldberger, A. L. (1994). Mosaic organization of DNA nucleotides. *Phys. Rev. E*, 49, 1685-1689, <https://doi.org/10.1103/PhysRevE.49.1685>.
- Prakash, S., Gupta, S. P., and Subbaraya, B. H. (1970). A study of the irregularities in the night time equatorial E-region using a Langmuir probe and plasma noise probe. *Planet. Space Sci.*, 18, 1307-1318, [https://doi.org/10.1016/0032-0633\(70\)90141-8](https://doi.org/10.1016/0032-0633(70)90141-8).
- Prakash, S. (1999). Production of electric field perturbations by gravity wave winds in the E region suitable for initiating equatorial spread F. *J. Geophys. Res.*, 104, 10051-10069, <https://doi.org/10.1029/1999JA900028>.
- Rino, C. L., Tsunoda, R. T., Petriceks, J., Livingston, R. C., Kelley, M. C., and Baker, K. D. (1981). Simultaneous rocket-borne beacon and in situ measurements of equatorial spread F-intermediate wavelength results. *J. Geophys. Res.*, 86, 2411-2420, <https://doi.org/10.1029/JA086iA04p02411>.
- Rodrigues, F. S., De Paula, E. R., and Chau, J. L. (2011). On the characteristics of 150-km echoes observed in the Brazilian longitude sector by the 30 MHz São Luís radar. *Ann. Geophys.*, 29, 1905-1916, <https://doi.org/10.5194/angeo-29-1905-2011>.
- Savio Odriozola, S., De Meneses, F. C. Jr., Muralikrishna, P., Pimenta A., and Kherani, E. (2017). Rocket in situ observation of equatorial plasma irregularities in the region between E and F layers over Brazil. *Ann. Geophys.*, 35, 413-422, <https://doi.org/10.5194/angeo-35-413-2017>.
- Sinha, H. S. S., Shikha, R., and Misra, R. N. (1999). First simultaneous in situ measurement of electron density and electric field fluctuations during spread F in the Indian zone. *Geophys. Res. Lett.*, 26, 1669-1672, <https://doi.org/10.1029/1999GL900339>.
- Sinha, H. S. S., Pandey, R., and Misra, R. N. (2010). In situ measurement of

- nighttime plasma density irregularities over an equatorial station Trivandrum. *J. Geophys. Res.*, 115, A11308, <https://doi.org/10.1029/2010JA01561>.
- Sinha, H. S. S., Pandey, R., Sharma S., and Misra R. N. (2011). Nighttime E region plasma irregularities over an equatorial station Trivandrum. *J. Atmos. Sol-Terr. Phys.*, 73, 2444-2452, <https://doi.org/10.1016/j.jastp.2011.10.005>.
- Spicher, A., Miloch, W. J., and Moen, J. I. (2014). Direct evidence of double-lobe power spectra in the highlatitude ionospheric plasma, *Geophys. Res. Lett.*, 41, 1406-1412, <https://doi.org/10.1002/2014GL059214>.
- Veronese, T. B., Rosa, R. R., Bolzan, M. J. A., Rocha Fernandes, F.C., Sawant, H. S., Karlický M. (2011). Fluctuation analysis of solar radio bursts associated with geoeffective X-class flares. *J. Atmos. Sol-Terr. Phys.*, 73, 1311-1316, <https://doi.org/10.1016/j.jastp.2010.09.030>.
- Vickrey, J. F., and Kelley, M. C. (1982). The effects of a conducting E layer on classical F region crossfield plasma diffusion. *J. Geophys. Res.*, 87, 4461-4468, <https://doi.org/10.1029/JA087iA06p04461>.
- Vickrey, J. F., Kelley, M. C., Pfaff, R., and Goldman, S. R. (1984). Lowaltitude image striations associated with bottomside equatorial spread F: Observations and theory. *J. Geophys. Res.*, 89, 2955-2961, <https://doi.org/10.1029/JA089iA05p02955>.
- Wakai, N. (1967). Quiet and disturbed structure and variations of the nighttime E region. *J. Geophys. Res.*, 72, 4507-4517, <https://doi.org/10.1029/JZ072i017p04507>.
- Yokoyama, T., Patra, A. K., Fukao, S., and Yamamoto, M. (2005). Ionospheric irregularities in the low-latitude valley region observed with the Equatorial Atmosphere Radar. *J. Geophys. Res.*, 110, A10304, <https://doi.org/1029/2005JA011208>.

Table 1: DFA1 to DFA5 for downleg time series at  $\sim 143.03$  km.

DFA order	$\alpha 1$	$\alpha 2$
DFA1	0.39	1.50
DFA2	0.15	1.93
DFA3	0.12	2.08
DFA4	0.10	2.26
DFA5	0.13	2.53

Table 2: Comparison of PSD spectral indices ( $\beta$ ) found in previous equivalent studies and  $\beta$  obtained here from DFA. All results measured using rockets are related to electronic density measurements during the experiment.

Date and Time	Spacecraft	Altitude (km)	$\beta$ range	$\langle \beta \rangle$	$\sigma_m$	References
17/07/1979, 12:31:30 UT	Rocket	250 to 370	-1.20 to -3.4	-2.3	110%	Rino et al. (1981)
17/07/1979, 12:31:30 UT	Rocket	250 to 285	-2.00 to -3.4	-2.7	70%	Kelley et al. (1982)
11/12/1985, 00:30 UT	Rocket	210 to 306	-1.34 to -3.3	-2.32	98%	Muralikrishna and Vieira (2007)
31/10/1986, 03:00 UT	Rocket	100 to 220	-1.54 to -3.30	-2.42	88%	Muralikrishna and Vieira (2007)
14/10/1994, 22:55 UT	Rocket	117 to 518	-1.20 to -5.3	-3.25	205%	Muralikrishna and Vieira (2007)
18/12/1995, 00:17 UT	Rocket	240 to 500	-1.11 to -4.90	-3.01	189%	Muralikrishna and Vieira (2007)
15/01/2007, 16:43 UT	Rocket	- to 127	-1.60 to -2.70	-2.15	55%	Sinha et al. (2010)
29/01/2008, 15:49 UT	Rocket	- to 117	-2.00 to -3.50	-2.75	75%	Sinha et al. (2011)
08/12/2012, 22:00 UT	Rocket	- to 317	-0.98 to -2.14	-1.56	58%	This paper

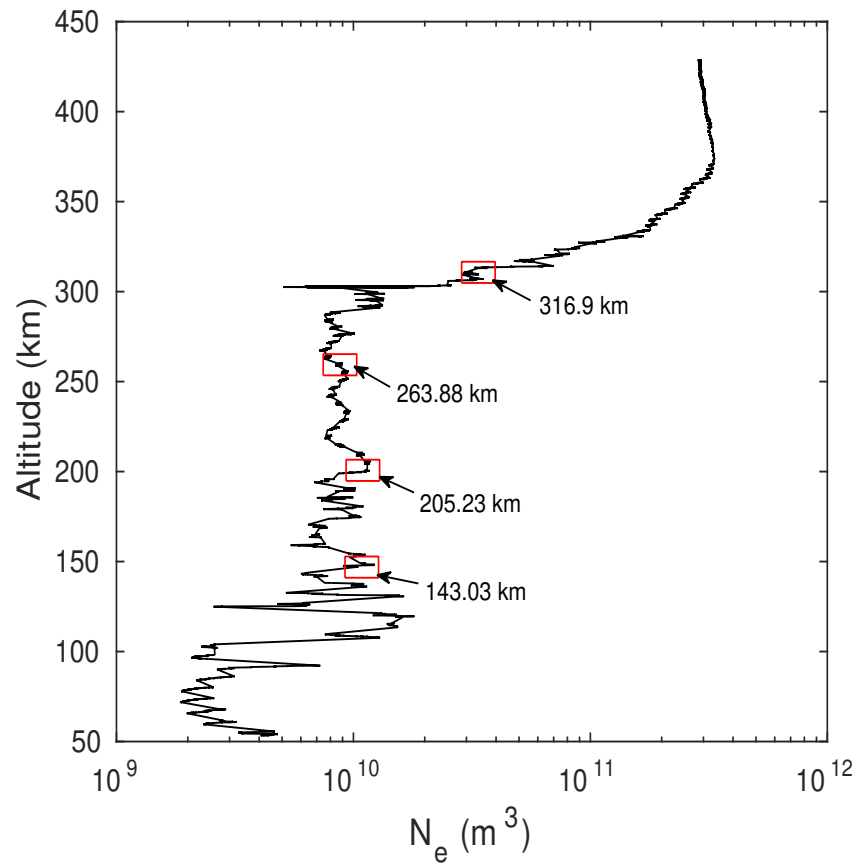


Figure 1: Vertical profile of electron densities for downleg trajectory. Open red boxes represent the chosen heights.

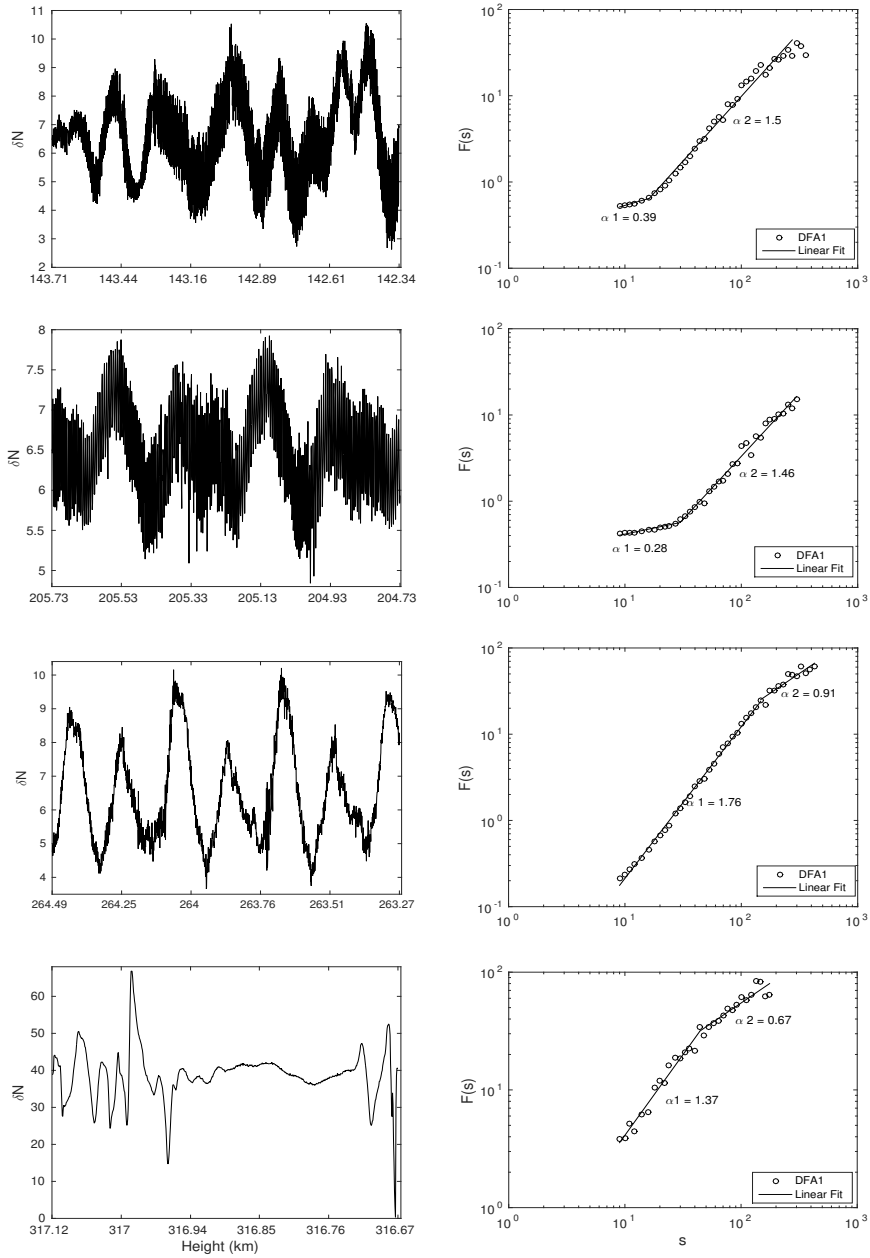


Figure 2: Left column - E-F valley region time series ( $\delta N$ ) of electron density fluctuations obtained from Langmuir probe during the downleg flight for the chosen heights. Right column - Corresponding fluctuation function profile  $F(s)$  (open circle) as a function of scales  $s$  along with the fit (solid line), i.e., the  $\alpha$  exponent.

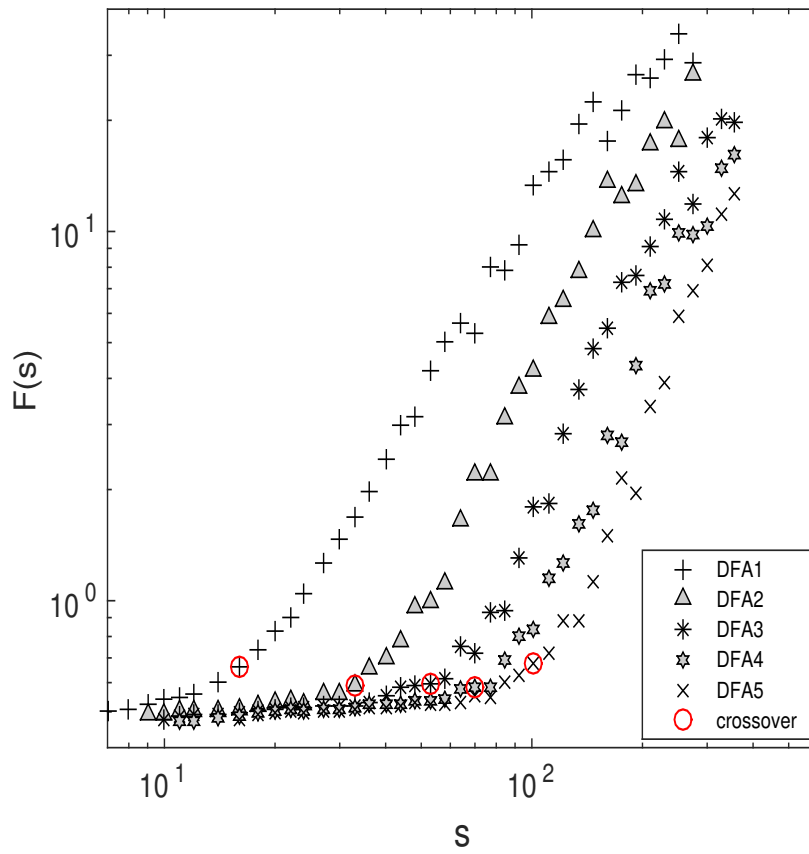


Figure 3: Fluctuation function profiles for the downleg time series at a mean height of 143 km for polynomials of orders 1-5. Open red circles represent the crossover points for the respective detrending order.

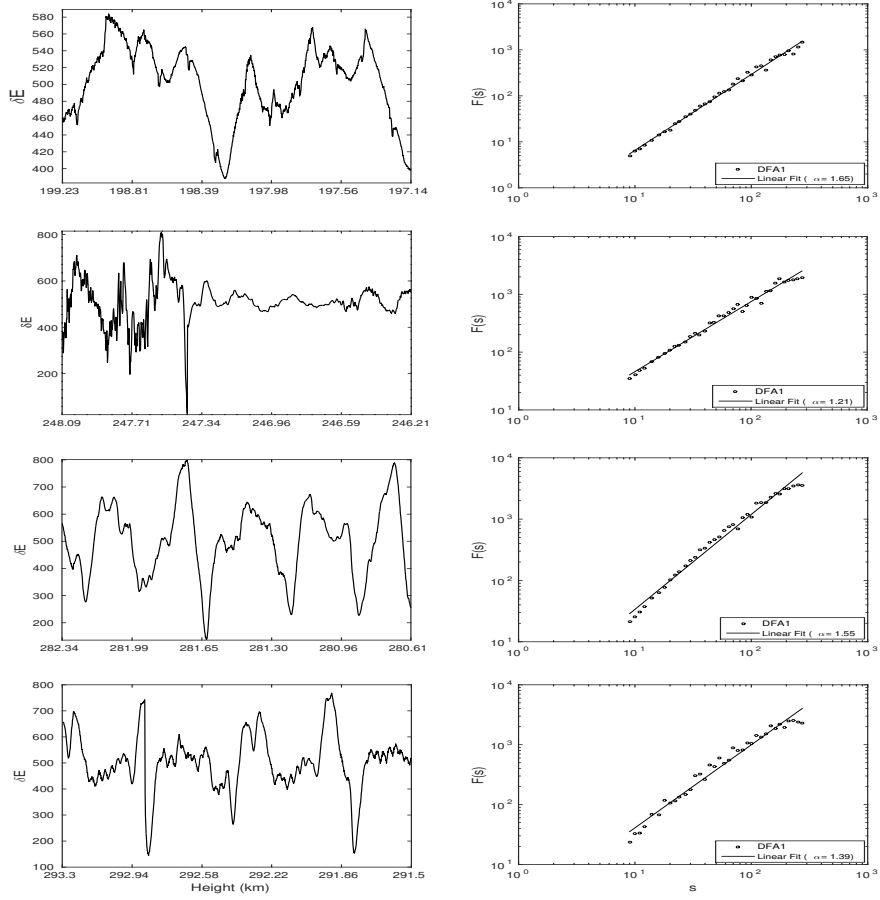


Figure 4: Left column - F region time series ( $\delta E$ ) of electric field fluctuations obtained from electric field probe during the downleg flight. Right column - Corresponding fluctuation function profile  $F(s)$  (open circle) as a function of scales  $s$  along with the fit (solid line), i.e., the  $\alpha$  exponent.

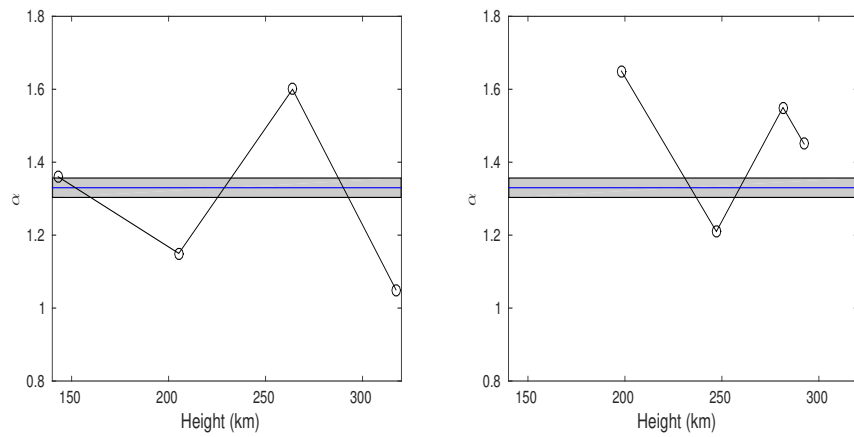


Figure 5: Mean height vs. DFA exponent  $\alpha$  for downleg plasma density fluctuation time series: E-F valley region (left) and F region (right). Solid line in the shaded area indicates the exponent value for homogeneous turbulence (k41 theory) with  $\beta = 1.66$ , i.e.,  $\alpha = 1.33$ ; shaded area shows the range of alpha value deviation  $\pm 2\%$ .